Gold nanoparticles-based multifunctional nanoconjugates for highly sensitive and enzyme-free detection of *E.coli* K12

Yongjin Zou, Jing Liang, Zhe She, Heinz-Bernhard Kraatz

www.elsevier.com/locate/talanta

PII: S0039-9140(18)30978-0
DOI: https://doi.org/10.1016/j.talanta.2018.09.068
Reference: TAL19082

To appear in: *Talanta*

Received date: 3 August 2018
Revised date: 17 September 2018
Accepted date: 18 September 2018

Cite this article as: Yongjin Zou, Jing Liang, Zhe She and Heinz-Bernhard Kraatz, Gold nanoparticles-based multifunctional nanoconjugates for highly sensitive and enzyme-free detection of *E.coli* K12, *Talanta,* https://doi.org/10.1016/j.talanta.2018.09.068

Gold nanoparticles-based multifunctional nanoconjugates for highly sensitive and enzyme-free detection of *E.coli* K12

Yongjin Zou[a,b], Jing Liang[a], Zhe She[b1], Heinz-Bernhard Kraatz[b,c*]

[a]*Guangxi Key Laboratory of Information Materials, Guilin University of Electronic Technology, Guilin 541004, P.R. China*

[b]*Department of Physical and Environmental Sciences, University of Toronto Scarborough, Toronto M1C 1A4, Canada*

[c]*Department of Chemistry, University of Toronto, M5S 3H6, Canada*

bernie.kraatz@utoronto.ca

ABSTRACT

Immobilization of proteins on a biocompatible conductive interface is highly desirable for the fabrication of biosensors. In this study, a nanocomposite has been prepared by assembling well-distributed gold nanoparticles (AuNPs) on the surface of a polypyrrole-reduced graphene oxide (PPy-rGO) composite through electrostatic adsorption. This serves as a platform for immobilization of a capture antibody, which was conjugated onto the ferrocene doped polypyrrole-gold nanoparticles (PPy@Fc/AuNPs) composite. The design and performance of the biosensor was tested against detection of a whole-cell bacteria *E. coli* K12. This nanocomposite has a high surface area, good conductivity and biocompatibility, which is shown to be very suitable for enzyme-free detection of this bacteria. Results show excellent analytical performance with a linear range from 1.0×10^{1} to 1.0×10^{7} CFU mL^{-1} and a low detection limit of 10 CFU mL^{-1}. The sensor has high selectivity, excellent

[1] *Current address: Department of Chemistry, Queen's University, K7L 3N6, Canada*

reproducibility, and good stability.

Keywords: Graphene; gold nanoparticles; *E.coli*; detection; immunosensor

1. Introduction

Accurate and robust detection of pathogenic bacteria in food and water remains an important issue. For the assessment of possible microorganism contamination of food, the number of *E.coli* is one of the most representative indicators [1]. That is because some of the strains of *E.coli* (O157:H7, etc.) are highly toxic and the infection dose is as low as 10 cells. The outbreaks of *E.coli* contamination have resulted in serious public health issues and numerous economic losses [2, 3]. According the estimation of World Health Organization (WHO), 1.5 million children lose their lives owing to the diarrheal diseases every year, 88% of which were caused by polluted drinking water with *E. coli* [4]. In the past decades, the methods for the detection of *E.coli* have been extensively explored, including culturing plate counting [5], enzyme-linked immunosorbent assay (ELISA)[6, 7], polymerase chain reaction (PCR) [8-10], field-effect transistor-based sensors [11]. Though reliable results can be obtained from these methods, the drawbacks includes time-consuming, labor-intensive, expensive instrumental, as well as skillful operator needed, which limit their applications mostly in a laboratory setting [12]. To meet the emerging challenges of fast and point-of-care testing, electrochemical biosensors offer unique opportunities by providing a simple route with many advantages including high sensitivity, good selectivity, wide linear range, potential miniaturization, and low cost [13]. Therefore, electrochemical analytical techniques have been a major direction in

the field.

In recent years, advances in nanotechnology have continued to drive new developments in the field of electrochemical biosensors. For example, signal amplification has been achieved with uses of smart nanoparticles [8, 14]. The idea is to take advantages of these nanomaterials, and exploit enhanced charge transfer, high surface area and create biocompatibility. Carbon-based nanomaterials [15, 16], gold nanoparticles [17-19], and conducting polymers [20, 21] have become popular and been used to high loading of binding tags and for the amplification of the electrochemical signal. Graphene is a two-dimensional single layer carbon nanosheet material, which has good conductivity and a high surface area [15, 22-24]. But its chemical inertness makes it difficult to attach proteins on the surface of graphene directly. The functionalization of graphene surfaces with other nanoparticles is a possible solution. But this brings problems associated with poor nanoparticle dispersion, as is the case for AuNPs [25]. Examples include Liang et al, who deposited AuNPs (>30 nm) by chemical reduction [26]. In other studies, graphene surfaces were decorated with AuNPs using polymers, such as Nafion [27] and poly(diallyldimethyl ammonium chloride) [25]. However, these did not solve the problems that AuNPs were decorated on the surface of graphene with low dispersion and the poor conductivity of these polymers in neutral solution reduced the performance of graphene. In essence, the decoration of graphene surfaces with AuNPs without reducing the conductive properties of the graphene construct remains a significant challenge.

In this study, we exploited polypyrrole (PPy) as a potential approach to achieve a disperse AuNPs distribution. PPy has good electrical conductivity, environmental

stability, and biocompatibility, and is an ideal substrate for nanoparticle modification [28]. Polymerization of pyrrole on graphene oxide in the presence of ammonium peroxydisulfate (APS) generates a positively charged surface. AuNPs, prepared using citrate as reducing agent, will carry a negative surface charge and decorate the surface of the positively charged PPy-graphene composite. The resulting nanocomposite, PPy-rGO/AuNPs, is then employed as biocompatible platform for the attachment of a capture antibody (Ab_1). The attachment of a peroxidase-labeled detection antibody (Ab_2) will allow the generation of an electrochemical signal in the presence of an analyte but it requires an electron mediator and H_2O_2 [29-31], Ferrocene (Fc)-labeling of the detection antibody is an effective way to generate a quantifiable current signal in sandwich assays [32-34].

In this work, the Fc redox label is encapsulated within the matrix of the PPy nanoparticles and used as an enzyme-free label to generate a current response. The preparation of PPy@Fc/AuNPs-Ab_2 label is shown in Scheme 1a and the preparation of an *E.coli* K12 immunosensor on graphene oxide surfaces is illustrated in Scheme 1b. AuNPs were attached on the PPy surface by electrostatic adsorption. The resulting sensor shows excellent sensitivity and selectivity, in addition to excellent stability.

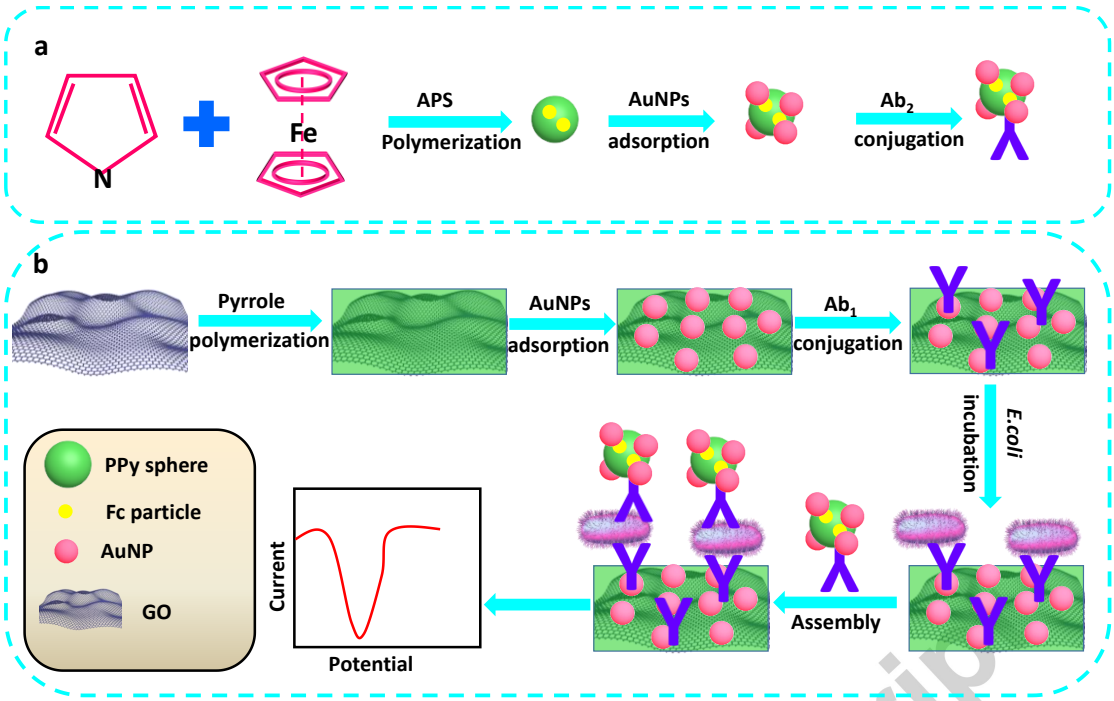

Scheme 1. Schematic illustration of the construction sensor surface and its use in the detection of *E.coli* K12: (a) construction of PPy@Fc/AuNPs-Ab_2 by pyrrole polymerization and doping with Fc, followed by Au NPs electrostatic adsorption and modification with Ab_2; (b) preparation of the PPy-rGO/AuNPs nanocomposite followed by Ab_1 attachment and detection of *E.coli* K12 employing a sandwich assay with PPy@Fc/AuNPs-Ab_2.

2. Material and methods

2.1. Chemicals and Materials

Pyrrole, gold chloride ($HAuCl_4$), sodium citrate, ferrocene, ammonium peroxydisulfate (APS) and potassium ferricyanide were obtained from Sigma-Aldrich (Oakville, ON). 1-Lipoic acid n-hydroxysuccinimide ester (LPA) was synthesized based on the established procedures [35]. All other chemicals are analytical grade and used as received. Deionized water was used to prepare all the solutions. Graphene oxide was prepared using Hummers' method [36]

and the negative charged colloidal AuNPs were prepared by citrate reduction, as reported before [37].

Polyclonal antibodies of E. coli serotype O/K were purchased from Thermo Fisher Scientific and diluted with phosphate buffered saline (PBS) (pH 7.4, 0.01 M phosphate, 0.14 M NaCl, 2.7 mM KCl). (It should be noted here that polyclonal antibodies of *E. coli* was used as both capture antibody (Ab_1) and detection antibody (Ab_2) because the monoclonal antibody for *E.coli* K12 is not commercial available. the size of *E.coli* K12 (several microns) much larger than that of antibody (about 10 nm), spatially, the binding site of *E.coli* K12 can not be occupied by Ab_1 completely. Therefore, in the following text, both Ab_1 and Ab_2 are referred to polyclonal antibodies of *E.coli* K12). The *E.coli* K12 was grown in lysogeny broth (LB) at 37 ºC, and then collected and killed with 4% PFA. Optical density at 600 nm (OD600) was measured and adjusted to around 0.60, which corresponds to the bacteria concentration of 1.0×10^8 CFU mL^{-1}.

2.2 Preparation of PPy-rGO/AuNPs nanocomposite and PPy@Fc/AuNPs antibody label

Graphene oxide (0.5 g) was first added to 100 mL deionized water and ultrasonicated for 1 h. Next, 0.25 mL of pyrrole and 0.01 mL of HCl (37 wt%) was added to the above suspension and stirred for 1 h. Thereafter, 10 mL of APS (0.2 g mL^{-1}) was added to the mixture in a dropwise manner under vigorously stirring. The mixture was further stirred for 4 h and then 100 mL of colloidal AuNPs was mixed with the above solution. Finally, the black suspension was centrifuged, rinsed with methanol and water thoroughly, and then dried in the

oven at 60 ºC for 12 h. The black power was identified as PPy-rGO/AuNPs. For comparison, PPy-rGO was prepared under identical condition without the mixing of colloidal AuNPs solution.

PPy@Fc/AuNPs was prepared with similar procedure. Briefly, pyrrole (0.25 mL), HCl (0.01mL) and sodium dodecyl sulfate (0.01 g) were dissolved in 100 mL deionized water and stirred for 1 h. Next, 0.5 g of Fc was dissolved in 10 mL of ethanol and added to solution dropwise and stirred for 1 h (Please note that Fc was not dissolved in water, therefore, it should be dissolved in ethanol first.). Subsequently, APS and colloidal AuNPs were added to above solution with same concentration and procedure as the preparation of PPy-rGO/AuNPs nanocomposite. Finally, the suspension was centrifuged, rinsed with water thoroughly. The black powder was then dried in the oven at 60 ºC for 12 h. The FTIR spectra of Fc, PPy, and PPy@Fc were shown in Fig.S1. The results indicate the Fc was successfully doped in the PPy nanosphere (See supporting information for more details).

The Ab_2 was bound on the PPy@Fc/AuNPs surface using LPA as linker according our previous work [38]. In detail, the 0.1 g of PPy@Fc/AuNPs was dispersed in 1 mL of LPA (0.01 M in ethanol solution) to form a self-assembled monolayer and the mixture was kept at 4 °C for 4 h. Then PPy@Fc/AuNPs nanocomposite was centrifuged, rinsed with water. The PPy@Fc/AuNPs nanocomposite was then incubated in Ab_2 (0.2 mg mL^{-1}) solution for 12 h (denoted as PPy@Fc/AuNPs-Ab_2), then rinsed with PBS and dispersed in 1 mL of PBS to form homogeneous dispersions. Finally, the PPy@Fc/AuNPs-Ab_2 label was stored in refrigerator at 4 ºC for use.

2.3 Preparation of the E.coli immunosensor

PPy-rGO/AuNPs nanocomposite was first suspended in N,N dimethylformamide (DMF) at a concentration of 0.3 mg mL^{-1} by ultrasonication for 1 h. Then 3 μL (about one drop) of the suspension was dropped on the surface of a cleaned glassy carbon electrode ([39] and dried at room temperature. Then the modified electrode was incubated in 0.01 M LPA solution for 4 h, rinsed with PBS and blocked with 3wt% bovine serum albumin (BSA) solution. Then the electrode was incubated in Ab_1 solution (0.2 mg mL^{-1}) for 4h. Finally, the electrode was rinsed again with PBS and kept at 4 ºC for use.

To detect *E.coli* K12, the PPy-rGO/AuNPs nanocomposite modified electrode was incubated a series of *E. coli* K12 suspension with cell concentrations ranging 1.0×10^1–1.0×10^7 CFU mL^{-1} at 4 ºC for 2 h. Then the electrode was rinsed with PBS to remove the physically attached cells. Finally the electrode was incubated in PPy@Fc/AuNPs-Ab_2 suspension for 2h. After rinsed with PBS, the electrode was ready for measurement.

2.4. Apparatus

The Fourier transform infrared (FTIR) spectra of the samples were recorded using an IR Nicolet 6700 spectrometer. Powder X-ray diffraction (XRD) (1820, Philips, The Netherlands) was performed with Cu K_α radiation (λ = 1.5418 Å). The Raman spectra were recorded by a Renishaw Invia Raman microscope system (Renishaw, Britain) with 633-nm laser excitation source. The N_2 adsorption−desorption isotherms were recorded by a Quantachrome Autosorb-iQ2 Automated gas sorption system at 77 K. The specific surface areas were calculated

using the Brunauer–Emmett–Teller (BET) method. The morphology of the nanoparticles was characterized using a transmission electron microscope (TEM, Tecnai G2 F20 S-TWIN, FEI). The electrochemical tests were performed on an electrochemical station (CHI instruments, USA) using a three-electrode configuration in PBS solution at room temperature. Differential pulse voltammetry (DPV) was employed for the detection over a potential range of 0 to 0.4 V versus Ag/AgCl. The PPy-rGO/AuNPs nanocomposite modified glassy carbon electrode described above served as working electrode. Ag/AgCl and platinum wire were used as the reference and counter electrodes, respectively.

3. Results and discussion

3.1 Characterization of the PPy-rGO/AuNPs nanocomposite

The nanocomposite was investigated by FTIR shown in Fig.1a. For the spectrum of GO, the peaks located at 3432 and 1385 cm^{-1} are assigned to stretching vibration and deformation vibration of O–H group, respectively [40]. The peak at 1112 cm^{-1} is attributed to the C–O stretching vibration while the peak at 1734 cm^{-1} is indexed to the C=O stretching band [41]. These peaks become weaker and disappeared in the spectrum of PPy-rGO and PPy-rGO/AuNPs, which is due to reduction of the GO by pyrrole [28]. It is widely accepted that rGO shows better conductivity than GO [42]. Therefore, the reduced form of GO is more suited for the fabrication electrode materials. The peaks at 1562 and 3428 cm^{-1} in the spectrum of PPy-rGO are attributed to the C–C and N–H stretching vibrations, respectively, while the peaks at 1183 cm^{-1} correspond to the C–N bending modes in the PPy ring [40], indicating that PPy was successfully deposited on the graphene surface. No obvious difference was

observed in the spectra of PPy-rGO and PPy-rGO/AuNPs, which indicated AuNPs was physically attached on the surface of PPy-rGO.

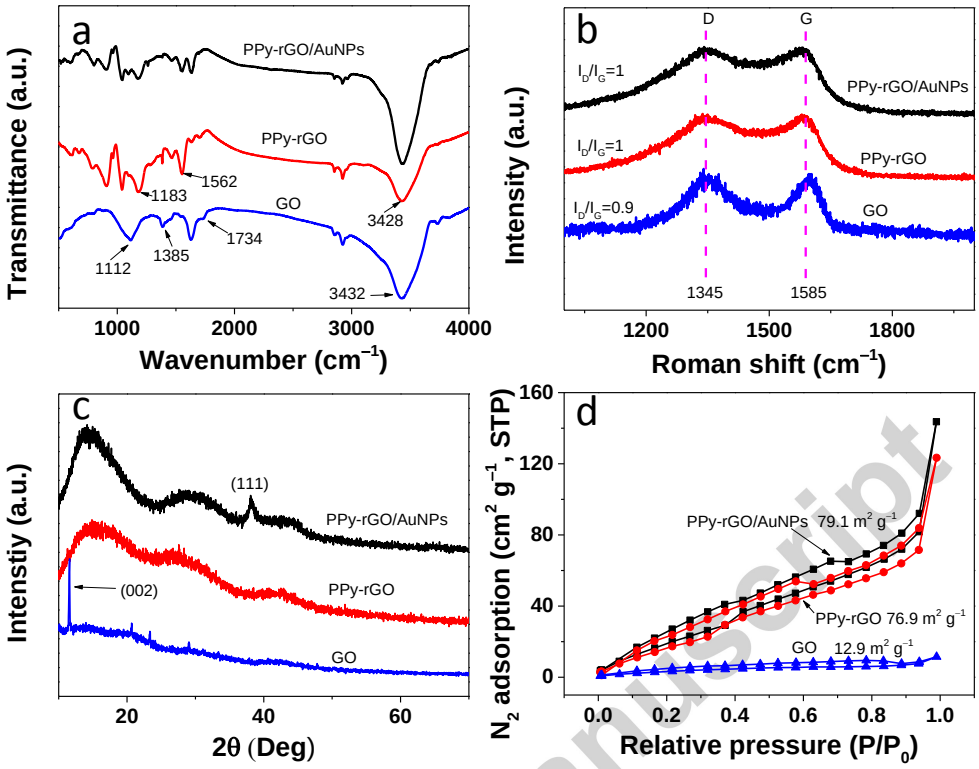

Fig.1. (a) FTIR spectra; (b) Raman spectra; (c) XRD patterns; (d) Nitrogen sorption isotherms for the sample of PPy-rGO/AuNPs, PPy-rGO and GO. Physicochemical characterizations confirm PPy-rGO/AuNPs nanocomposite was sucessfully prepared. AuNPs were physically attached on the PPy-rGO and PPy-rGO/AuNPs shows high surface area.

The samples were further studied by Raman spectroscopy. As shown in Fig. 1b, a graphite-like band (G-band) at 1585 cm^{-1} and a disorder-induced band (D-band) at 1345 cm^{-1} were observed in all the samples, suggesting the coexistence of disordered and graphitic carbons [43]. The change in the disorder level can be accessed by the peak intensity (I_D/I_G) ratio. GO shows a relatively low I_D/I_G ratio (0.9) in the present

study. In the sample of PPy-rGO and PPy-rGO/AuNPs, the D band becomes broad and I_D/I_G increased to 1.0, suggesting an increase of disorder level owing to the coating of PPy on GO. However, the assembly of AuNPs on the PPy-rGO did not change the I_D/I_G ratio. These results further confirm the successful polymerization of PPy on graphene nanosheets.

Fig.1c shows the XRD patterns of the sample of PPy-rGO/AuNPs, PPy-rGO and GO. A sharp peak at $2\theta = 10.5^o$ was observed in the pattern of GO, which corresponds to the diffraction of the (002) graphite oxide plane [28]. This peak disappeared in the patterns of PPy-rGO and PPy-rGO/AuNPs, which indicates the GO was completely reduced [41]. Two broad peaks centered at 22.2^o and 43.9^o are observed in the sample of PPy-rGO and PPy-rGO/AuNPs, repectively, which is due to the amorphous nature of PPy [44]. An additional peak at 38.1^o was found in the pattern of PPy-rGO/AuNPs when comparing with PPy-rGO, which is indexed to the (111) Bragg reflections of the face centered cubic structure (JCPDS no. 04-0783) of AuNPs [45]. The particle size calculated from Scherrer equation is about 7.3 nm [46]. These results indicate that AuNPs was successfully dispersed on the surface of PPy-rGO.

The surface area of the nanoparticles was examined by N_2 adsorption–desorption method. As shown in Fig.1d, the BET surface areas were 12.9, 76.9, and 79.1 $m^2\ g^{-1}$ for GO, PPy-rGO, and PPy-rGO/AuNPs, respectively. GO shows lowest surface area in the three samples, which is possibly due to the aggregation of the graphene nanosheets. After deposted PPy on the surface of GO, the surface area increased about more than 6 times, suggesting the PPy prevent the aggregation of the graphene nanosheets, which is because PPy is an effective capping agent to prevent the

restacking and form organically dispersible graphene [28]. The surface area increased slightly for the sample of PPy-rGO/AuNPs, which indicates the AuNPs do not block the pore the PPy-rGO nanocomposite. The isotherm of PPy-rGO/AuNPs is of type IV with a large hysteresis loop, attributing to the abundance of mesopores inside the material. A larger specific surface area affords more active sites for the immobilization of proteins and electron transfer, and hence amplifies the electrochemical signal. Therefore, PPy-rGO/AuNPs is expected to have better electrochemical perforance than that of GO and PPy-rGO.

The TEM images of the nanocomposites are shown in Fig.2. GO exhibits a wrinkled surface, which is the typical characterization of GO [47] (Fig.2a). After the deposition of PPy on the surface of GO, the surface becomes rough (Fig.2b). The AuNPs was uniformly distributed on the surface of PPy-rGO without obvious aggregation (Fig.2c). The diameter of AuNPs is about 10 nm, which is very similar to the size caculated from the XRD pattern. For comparasion, the AuNPs was attached on the surface of GO without the assitance of PPy, Fig. S2 shows that the AuNPs aggregated on the surface severly and the dispersion is rather poor. The PPy nanosphere displays interconnected sphere with a diamter of about 50 nm. When Fc was doped in the polypyrrole nanosphere, the shape does not change. Expectedly, AuNPs was assembled on the nanophere based on electrotatic adsorption. AuNPs can be well dispersed in the form of colliod due to the electrostatic repulsion [37]. However, it is caused severe aggregation on a solid surface due to high surface energy. In this study, a unque and simple method was developed to decorate AuNPs on the PPy surface uniformly, which provide an excellent interface for the protein immobilization.

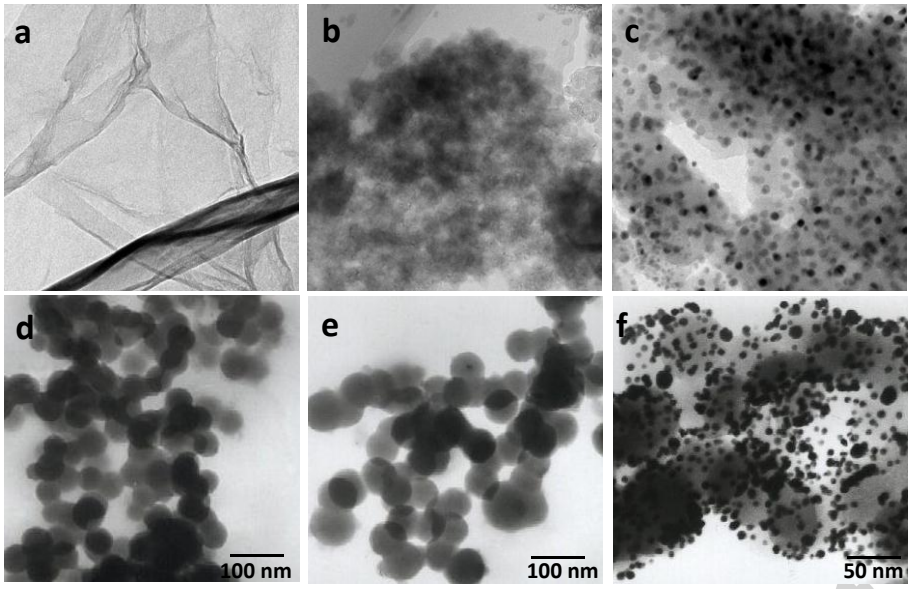

Fig.2. TEM iamges of (a) GO, (b)PPy-rGO, (c)PPy-rGO/AuNPs, (d)PPy nanosphere, (e) PPy@Fc and (d) PPy@Fc/AuNPs. The TEM images give direct evidence that the AuNPs are well distributed on the PPy-rGO and PPy@Fc substrates.

3.2 Electrochemical performance of the modified electrode

The electrochemical performance of the nanocomposite was investigated by cyclic voltammetry (CV) and electrochemical impedance spectroscopy (EIS) in a 2.5 mM/2.5 mM $Fe(CN)_6^{3-/4-}$ and 0.1 M KCl solution. Fig. 3a shows the CVs of the bare GCE, GO, PPy-rGO, PPy-rGO/AuNPs, PPy-rGO/AuNPs-Ab_1, PPy-rGO/AuNPs-Ab_1-E.coli electrodes obtained with a scan rate of 10 mV s^{-1}. It is clear to see that both the anodic and cathodic peak currents from GO and PPy-rGO modified electrodes are higher than that of bared GC electrode, indicating these surfaces are more effective for electron transfer. After the assembly of AuNPs on the surface of PPy-rGO, the peak currents decrease slightly due to the negatively charged surface of AuNPs [48], but are still higher than that of GC electrode. The peak currents of the electrode dropped dramatically after the conjugation of the Ab_1 on the surface of PPy-rGO/AuNPs, as a result of the insulating properties of the antibody.

The peak currents further dropped upon *E.coli* K12 binding to the modified electrode surface, which is attributed to the surface of the barrier provokes electrical charge redistribution and reduces the surface conductivity because of the bacteria binding.

The EIS curves of the electrodes were showed in Fig. 3b. The electron transfer resistance (R_{ct}) is calculated to be 500 Ω at the bare GC electrode through equivalent circuit simulation (Fig.S3). The R_{ct} decreases to 100 and 50 Ω for GC modified with GO and PPy-rGO, respectively, which suggests that the GO and rGO-PPy form high electron conduction pathways between the electrode and electrolyte. The R_{ct} increased significantly when the protein Ab_1 and *E.coli* was immobilized onto PPy-rGO/AuNPs electrode due to the block of the electron transfer by these molecules and cells. These results are consistent with CV observation.

The redox signals of Fc in PPy@Fc/AuNPs were investigated as CVs shown in Fig.3c. No redox peaks were found from the PPy modified electrode. In the CV curve of PPy@Fc, a well-defined redox peaks was observed around 0.2 V. The separation of the anodic and cathodic peak potential is only 65 mV, which is close to the theoretical value (59 mV) of for one electron transfer process [49], indicating a rapid electron transfer. Compared with PPy@Fc electrode, the peak current of PPy@Fc/AuNPs further increased, which is due to the AuNPs facilitated the electron transfer [39]. When the scan rate increased from 10 to 200 mV s^{-1}, the shape of the CV was well kept and separation of the peak potential increase slightly (Fig.3d), suggesting the good stability of PPy@Fc/AuNPs. The current is linearly increased with the scan rates (Fig.S4), suggesting the Fc signals are from immobilized Fc.

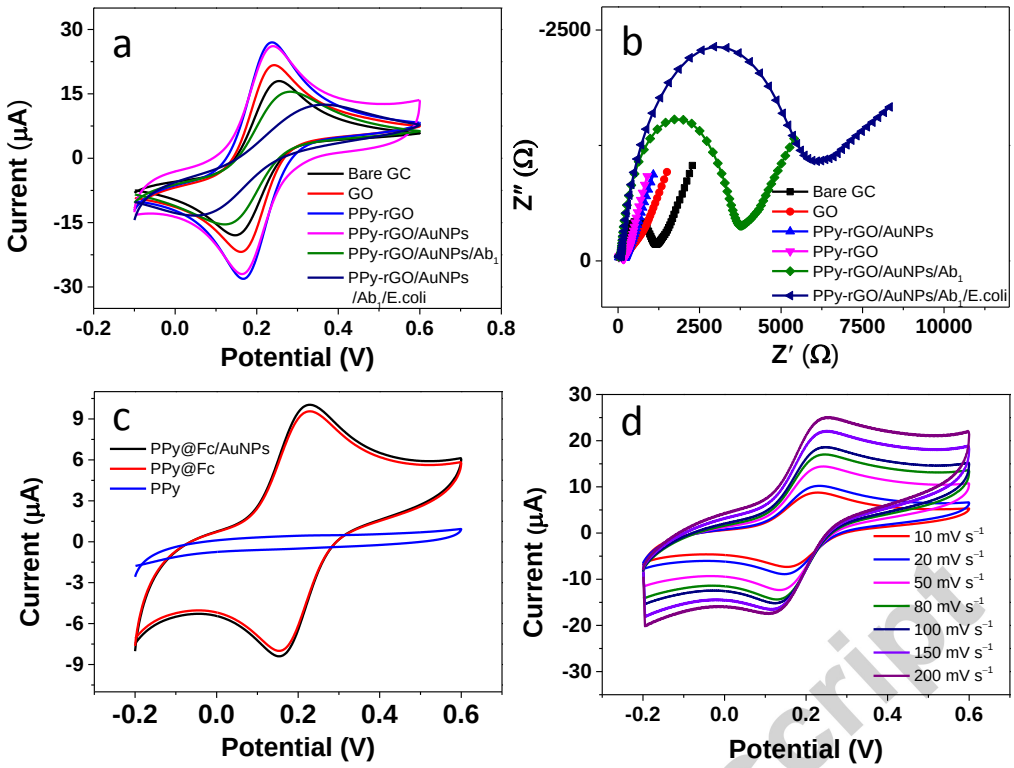

Fig.3. Electrochemical characterization of the prepared materials. CV (a) and EIS (b) curves of the electrode after each step modification at a scan rate of 10 mV s^{-1} in a 2.5 mM/2.5 mM $Fe(CN)_6^{3-/4-}$ and 0.1 M KCl solution. Impedance results were recorded from 100 kHz to 0.1 Hz. The CV and EIS curves indicate PPy-rGO/AuNPs shows best electrochemical performance and *E.coli* can be attached on the proposed electrode; (c) CV curves of PPy@Fc/AuNPs, PPy@Fc and PPy modified electrode at a scan rate of 10 mV s^{-1} in a 10 mM PBS solution; (d) CV curves of PPy@Fc/AuNPs at different scan rates in a 10 mM PBS solution. The CV curves of PPy@Fc/AuNPs indicate Fc was successfully doped in the PPy nanosphere.

3.3. Performance of the immunoassay to E.coli K12

Due to the rapid electron transfer and reverserable reaction, Fc is always used as the electrochemical probe. When the bacteria are bound to a modified surface, the surface conductivity is reduced. Therefore, a decrease in the heterogeneous rate constant of the redox active ion is observed. Thus the current signal can be monitored

for the detection of the bacteria. Before the detection of *E.coli* K12, a series of control experiments on the immunosensor were carried out. The effect of the PPy-rGO/AuNPs loading on the current response of the immunosensor to 1.0×10^4 CFU mL^{-1} of *E.coli* K12 was examined by varying the concentration of the dispersion solution from 0.1 to 0.5 g mL^{-1}. As shown in Fig.S5, the current response increased with the increasing of PPy-rGO/AuNPs concentration. The maximum and optimal value was reached at the concentration of 0.3 g mL^{-1}.

As showed in Fig. S6, with increasing the Ab_1 concentration, the current response increased and trended to the plateau value at the concentration of 0.2 mg mL^{-1} for Ab_1. Thus, 0.2 mg mL^{-1} Ab_1 was thus used for the preparation of immunosensor.

The effect of *E.coli* K12 incubation time on the analytical performance of immunoassay was also investigated. The current response for *E.coli* K12 immunosensor increased with increasing incubation time and trended to a constant value after an incubation time of 2 h (Fig. S7). The result showed a saturated binding between the analyte and the antibodies at 60 min, and longer incubation time did not obviously improve the response. Therefore, the incubation time of 2h was chosen as the optimal incubation condition for the immunoassay of *E.coli* K12.

Since the Fc is not soluble in aqueous solution and has a good redox reaction on the electrode, it was encapsulated in PPy nanospere to generate the current signal. The concentration of PPy@Fc/AuNPs-Ab_2 was varied to obtain the maximum current response. As shown in Fig. S8, the maximum current was reached at the concentration of 0.3 g mL^{-1}, which was selected for the final design.

The ionic strength of the PBS buffer is also investigated with the aim of improving the sensitivity of the immunosensor. Several concentrations were examined for this purpose. 1×PBS was 0.01 M phosphate, 0.14 M NaCl, 2.7 mM KCl solution. 2×PBS, 3×PBS, and 4×PBS is 2, 3 and 4 times concentrated 1×PBS. The experiment shows that varying ionic strength of the solution did not change the electrochemical

responses as shown in Figure S9. Since no effects of ionic strength were observed, standard 1×PBS was employed for the detection of *E.coli* K12.

Under the optimized condition, the current response of the immunosensor to varied concentrations of *E.coli* K12 in PBS solution was investigated as shown in Fig.4a. The peak current of the DPV curve in Fig. 4b increased with the increasing of the *E.coli* K12 concentration. The peak current increased linearly with the logarithm *E.coli* K12 concentration in the range from 1.0×10^{1} to 1.0×10^{7} CFU mL^{-1} with a correlation coefficient of 0.998 (Fig.4c). The detection limit calculated by the reported equation [50] is 10 CFU mL^{-1}. The analytical performance of the proposed method was compared with these nanomaterials based immunosensor for the detection of *E.coli* K12. As listed in Table 1, the linear range and detection limit are comparable with the previous reports, which indicate that immunosensor shows excellent performance. The good performance could be attributed to the signal amplification ability of PPy@Fc/AuNPs nanoparticles and promoted electron transfer on the electrode. Moreover, PPy-rGO/AuNPs with good biocompatibility is favorable to maintain the active configuration of the immunocomplex.

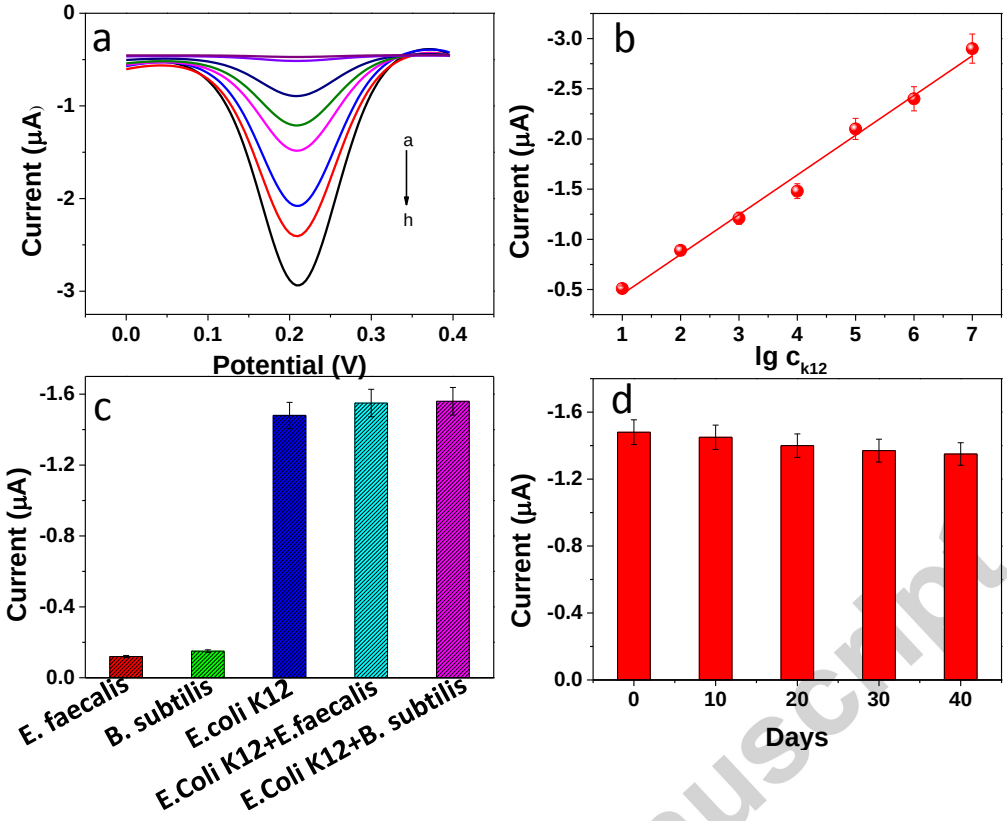

Fig.4 (a) DPV curves with varied *E.coli* K12 concentrations a, b, c, d, e, f, g and h to 0, 1.0×10^{1}, 1.0×10^{2}, 1.0×10^{3}, 1.0×10^{4}, 1.0×10^{5}, 1.0×10^{6} and 1.0×10^{7} CFU mL^{-1}, respectively; (b) calibration curve of the electrochemical immunosensor toward detection of *E.coli* K12; (c) The current response for *E. faecalis* (1.0×10^{4} CFU mL^{-1}), *E.coli* K12 (1.0×10^{4} CFU mL^{-1}), and *E. faecalis* (1.0×10^{4} CFU mL^{-1}) and *E.coli* K12 (1.0×10^{4} CFU mL^{-1}) in 0.1 M PBS solution; (d) Current response of the immunosensor to *E.coli* K12 (1.0×10^{4} CFU mL^{-1}) recorded from five identical electrodes at a time interval 10 days.

Table 1. Comparison between the proposed method and the reported immunosensor for the detection of *E.coli* K12

Immunosensor platform	**Bio-receptor of immobilization**	**Detection limit (CFU mL^{-1})**	**Linear range (CFU mL^{-1})**	**Ref.**
Electrochemical	Antibody	1.0×10^{2}	1.0×10^{2}–1.0×10^{6}	[12]

PCR	DNA	1.0×10^{3}	1.0×10^{1}–1.0×10^{7}	[51]
Electrochemical	Antibody	1.0×10^{2}	1.0×10^{2}–1.0×10^{5}	[52]
Fluorescence	Bacteriophage	-	1.0×10^{4}–1.0×10^{5}	[53]
Spectroscopy	Antibody	1.0×10^{1}	1.0×10^{1}–1.0×10^{7}	[54]
Optical	Antibody	1.0×10^{3}	1.0×10^{3}–1.0×10^{5}	[55]
Gravimetric	Antibody	1.0×10^{3}	1.0×10^{5}–6.2×10^{7}	[56]
Electrochemical	Antibody	1.0×10^{1}	1.0×10^{1}-1.0×10^{7}	This study

3.4. Selectivity, reproducibility and stability

To assess the selectivity of the proposed immunosensor, the *Enterococcus faecalis* (*E. faecalis*) (1.0×10^{4} CFU mL^{-1}), *Bacillus subtilis* (*B. subtilis*) (1.0×10^{4} CFU mL^{-1}) and mixed cultures with *E.coli* K12 (1.0×10^{4} CFU mL^{-1}) were evaluated. As shown in Fig.4d, the current signal for *E. faecalis* and *B. subtilis* were 0.2 and 0.15 μA, respectively, which is significantly lower than that of *E.coli* K12 (1.48 μA) . For the mixed culture, the current response recovered due to the addition of *E.coli* K12. These results demonstrate that the immunosensor has good selectivity and can perform well in a mixed cell culture. The most common electrochemical interfering species, such as ascorbic acid, uric acid and glucose were also examined. Individual compound was added to respective solution at a concentration of 0.1 mM. As shown in Fig.S10, no obvious current increase was observed in the immunosensor's response and the sensor is not influenced by the presence of these interfering species.

The reproducibility of the immunosensor was investigated by repeating with five different electrodes for the detection of 1.0×10^{4} CFU mL^{-1} of *E.coli* K12. The relative standard deviation (RSD) of the measurements for the five electrodes was 2.6%. The good reproducibility could be due to the unique preparation of the label and the immunosensor construction methods.

Similar test was also performed but using a batch of five electrodes prepared and stored in the refrigerator at 4 ºC. The electrode was tested to 1.0×10^{4} CFU mL^{-1} of *E.coli* K12 in a time interval of 10 days (Fig.4e). The electrochemical response was found to decrease by only 8.8% even after 40 days, indicating that the sensor surface is very stable.

3.5. Real sample testing

The performance of the immunosensors in the real-to-life conditions was investigated by standard addition method. Water and milk samples were spiked with *E.coli* K12. 0.1 M KCl was added to the solution and used as the supporting electrolyte. The results of five independent samples are given in Table 2. The obtained average recoveries of the proposed method for *E.coli* K12 were in the range of 96–104%. These results demonstrate the immunosensors with these nanocomposites are suitable for real sample analysis.

Table 2. Comparison of the proposed detection immunosensor assay and plate counting methods.

Samples	Number	Added (CFU mL^{-1})	Detected (CFU mL^{-1})	Average recovery
Tap water (City of Toronto)	1	$(1.5\pm0.1)\times10^4$	$(1.5\pm0.1)\times10^4$	100%
	2	$(2.5\pm0.2)\times10^4$	$(2.6\pm0.1)\times10^4$	104%
	3	$(4.0\pm0.3)\times10^4$	$(4.1\pm0.2)\times10^4$	102%
	4	$(5.0\pm0.1)\times10^4$	$(4.8\pm0.1)\times10^4$	96%
	5	$(8.0\pm0.1)\times10^4$	$(8.1\pm0.2)\times10^4$	101%
Milk (Grocery Store, Toronto)	1	$(2.0\pm0.1)\times10^4$	$(2.1\pm0.1)\times10^4$	105%
	2	$(3.5\pm0.2)\times10^4$	$(3.4\pm0.2)\times10^4$	97%
	3	$(5.0\pm0.1)\times10^4$	$(4.7\pm0.1)\times10^4$	94%
	4	$(6.0\pm0.3)\times10^4$	$(5.9\pm0.1)\times10^4$	98%
	5	$(7.5\pm0.3)\times10^4$	$(7.2\pm0.2)\times10^4$	96%

Conclusions

A simple method was proposed to disperse AuNPs on PPy surface uniformly. A highly sensitive sandwiched *E.coli* K12 immunosensor was constructed by using PPy-rGO/AuNPs as signal amplifier and PPy@Fc/AuNPs as signal generator. Due to the good conductivity and biocompatibility of the nanocomposite, the immunosensor exhibits excellent analytical performance even under real to life conditions. . Furthermore, the sensor has a dynamic range of 1.0×10^1 to 1.0×10^7 CFU

mL^{-1}, with a LOD of 10 CFU mL^{-1}. In addition, the sensor possesses good selectivity and excellent stability over an extended period. Testing of the sensor in real-to-life media (city water and milk) demonstrates that this approach is useful and should allow us to further develop this sensor into a practical device.

Acknowledgments

We appreciate funding from Natural Sciences and Engineering Research Council of Canada. Y.Z. was supported by the visiting scholars program of China Scholarship Council (CSC).

References

[1] Z. Altintas, M. Akgun, G. Kokturk, Y. Uludag, A fully automated microfluidic-based electrochemical sensor for real-time bacteria detection, Biosens. Bioelectron. 100 (2018) 541–548.

[2] F. Huang, H. Zhang, L. Wang, W. Lai, J. Lin, A sensitive biosensor using double-layer capillary based immunomagnetic separation and invertase-nanocluster based signal amplification for rapid detection of foodborne pathogen, Biosens. Bioelectron. 100 (2018) 583–590.

[3] S. Brosel-Oliu, R. Ferreira, N. Uria, N. Abramova, R. Gargallo, F.-X. Muñoz-Pascual, A. Bratov, Novel impedimetric aptasensor for label-free detection of Escherichia coli O157:H7, Sens. Actuators B: Chem. 255 (2018) 2988–2995.

[4] Y. Wen, L. Wang, L. Xu, L. Li, S. Ren, C. Cao, N. Jia, A. Aldalbahi, S. Song, J. Shi, J. Xia, G. Liu, X. Zuo, Electrochemical detection of PCR amplicons of Escherichia coli genome based on DNA nanostructural probes and polyHRP enzyme, Analyst 141 (2016) 5304–5310.

[5] K.S. Gracias, J.L. McKillip, A review of conventional detection and enumeration methods for pathogenic bacteria in food, Can. J. Microbiol. 50(2004) 883–890.

[6] B. Pang, C. Zhao, L. Li, X. Song, K. Xu, J. Wang, Y. Liu, K. Fu, H. Bao, D. Song, X. Meng, X. Qu, Z. Zhang, J. Li, Development of a low-cost paper-based ELISA method for rapid *Escherichia coli* O157:H7 detection, Anal. Biochem. 542 (2018) 58–62.

[7] C.M. Shih, C.L. Chang, M.Y. Hsu, J.Y. Lin, C.M. Kuan, H.K. Wang, C.T. Huang, M.C. Chung, K.C. Huang, C.E. Hsu, C.Y. Wang, Y.C. Shen, C.M. Cheng, Paper-based ELISA to rapidly detect *Escherichia coli*, Talanta 145 (2015) 2–5.

[8] Y. Zhou, A. Marar, P. Kner, R.P. Ramasamy, Charge-directed immobilization of bacteriophage on nanostructured electrode for whole-cell electrochemical biosensors, Anal. Chem. 89 (2017) 5734–5741.

[9] Y. You, S. Lim, J. Hahn, Y.J. Choi, S. Gunasekaran, Bifunctional linker-based immunosensing for rapid and visible detection of bacteria in real matrices, Biosens. Bioelectron. 100 (2018) 389–395.

[10] Y. Liu, P. Singh, A. Mustapha, High-resolution melt curve PCR assay for specific detection of *E. coli* O157:H7 in beef, Food Control 86 (2018) 275-282.

[11] S. Mao, J.B. Chang, G.H. Zhou, J.H. Chen, Nanomaterial-enabled rapid detection of water contaminants, Small 11(2015) 5336–5359.

[12] F. Moghtader, G. Congur, H.M. Zareie, A. Erdem, E. Piskin, Impedimetric detection of pathogenic bacteria with bacteriophages using gold nanorod deposited graphite electrodes, RSC Adv. 6(2016) 97832–97839.

[13] C.M. Pandey, I. Tiwari, V.N. Singh, K.N. Sood, G. Sumana, B.D. Malhotra, Highly sensitive electrochemical immunosensor based on graphene-wrapped copper oxide-cysteine hierarchical structure for detection of pathogenic bacteria, Sens. Actuators B: Chem. 238 (2017) 1060–1069.

[14] M. Sedki, R.Y.A. Hassan, A. Hefnawy, I.M. El-Sherbiny, Sensing of bacterial cell viability using nanostructured bioelectrochemical system: rGO-hyperbranched chitosan nanocomposite as a novel microbial sensor platform, Sens. Actuators B: Chem. 252 (2017) 191–200.

[15] N. Zainudin, A.R. Mohd Hairul, M.M. Yusoff, L.L. Tan, K.F. Chong, Impedimetric graphene-based biosensor for the detection of Escherichia coli DNA, Anal. Meth. 6(2014) 7935–7941.

[16] P. Subramanian, F. Barka-Bouaifel, J. Bouckaert, N. Yamakawa, R. Boukherroub, S. Szunerits, Graphene-coated surface plasmon resonance interfaces for studying the interactions between bacteria and surfaces, ACS Appl. Mater. Interfaces 6(2014) 5422–5431.

[17] A.R. Hassan, A. de la Escosura-Muniz, A. Merkoci, Highly sensitive and rapid determination of *Escherichia coli* O157:H7 in minced beef and water using electrocatalytic gold nanoparticle tags, Biosens. Bioelectron. 67 (2015) 511–515.

[18] Y.H. Lin, S.H. Chen, Y.C. Chuang, Y.C. Lu, T.Y. Shen, C.A. Chang, C.S. Lin, Disposable amperometric immunosensing strips fabricated by Au nanoparticles-modified screen-printed carbon electrodes for the detection of foodborne pathogen *Escherichia coli* O157:H7, Biosens. Bioelectron. 23(2008) 1832–1837.

[19] H.J. Liu, Y.Q. Teng, X.A. Zhang, Y. Fu, W. Zhang, L.T. Jin, Fe_3O_4@Au nanoparticles as labels for electrochemical immunodetection of *E. coli* in water, Chem. J. Chin. Univ. Chin. 31(2010) 1131–1136.

[20] E.B. Setterington, E.C. Alocilja, Rapid electrochemical detection of polyaniline-labeled *Escherichia coli* O157:H7, Biosens. Bioelectron. 26(2011) 2208–2214.

[21] A.D. Chowdhury, A. De, C.R. Chaudhuri, K. Bandyopadhyay, P. Sen, Label free polyaniline based impedimetric biosensor for detection of *E. coli* O157:H7 bacteria, Sens. Actuators B: Chem. 171–172 (2012) 916–923.

[22] Y. Li, J. Deng, L. Fang, K. Yu, H. Huang, L. Jiang, W. Liang, J. Zheng, A novel electrochemical DNA biosensor based on HRP-mimicking hemin/G-quadruplex wrapped GOx nanocomposites as tag for detection of *Escherichia coli* O157:H7, Biosens. Bioelectron. 63 (2015) 1–6.

[23] Y. Wang, J. Ping, Z. Ye, J. Wu, Y. Ying, Impedimetric immunosensor based on gold nanoparticles modified graphene paper for label-free detection of *Escherichia coli* O157:H7, Biosens. Bioelectron. 49 (2013) 492-498.

[24] I. Tiwari, M. Singh, C.M. Pandey, G. Sumana, Electrochemical detection of a pathogenic Escherichia coli specific DNA sequence based on a graphene oxide–chitosan composite decorated with nickel ferrite nanoparticles, RSC Adv. 5 (2015) 67115–67124.

[25] X. Zhang, Y. Jiang, C. Huang, J. Shen, X. Dong, G. Chen, W. Zhang, Functionalized nanocomposites with the optimal graphene oxide/Au ratio for amplified immunoassay of *E. coli* to estimate quality deterioration in dairy product, Biosens. Bioelectron. 89 (2017) 913–918.

[26] J. Liang, Z. Chen, L. Guo, L. Li, Electrochemical sensing of L-histidine based on structure-switching DNAzymes and gold nanoparticle-graphene nanosheet composites, Chem. Commun. 47 (2011) 5476–5478.

[27] S.S.J. Aravind, T.T. Baby, T. Arockiadoss, R.B. Rakhi, S. Ramaprabhu, A cholesterol biosensor based on gold nanoparticles decorated functionalized graphene nanoplatelets, Thin Solid Films 519 (2011) 5667–5672.

[28] C.A. Amarnath, C.E. Hong, N.H. Kim, B.C. Ku, T. Kuila, J.H. Lee, Efficient synthesis of graphene sheets using pyrrole as a reducing agent, Carbon 49 (2011) 3497–3502.

[29] X. Zhang, J. Shen, H. Ma, Y. Jiang, C. Huang, E. Han, B. Yao, Y. He, Optimized dendrimer-encapsulated gold nanoparticles and enhanced carbon nanotube nanoprobes for amplified electrochemical immunoassay of *E. coli* in dairy product based on enzymatically induced deposition of polyaniline, Biosens. Bioelectron. 80 (2016) 666–673.

[30] M. Xu, R. Wang, Y. Li, Electrochemical biosensors for rapid detection of *Escherichia coli* O157:H7, Talanta 162 (2017) 511–522.

[31] X. Zhang, W. Lu, E. Han, S. Wang, J. Shen, Hybrid Nanostructure-based

immunosensing for electrochemical assay of *Escherichia coli* as indicator bacteria relevant to the recycling of urban sludge, Electrochim. Acta 141 (2014) 384–390.

[32] B. Seiwert, U. Karst, Ferrocene-based derivatization in analytical chemistry, Anal. Bioanal. Chem. 390 (2008) 181–200.

[33] G. Wang, X. Gang, X. Zhou, G. Zhang, H. Huang, X. Zhang, L. Wang, Electrochemical immunosensor with graphene/gold nanoparticles platform and ferrocene derivatives label, Talanta 103 (2013) 75–80.

[34] J.D. Qiu, R.P. Liang, R. Wang, L.X. Fan, Y.W. Chen, X.H. Xia, A label-free amperometric immunosensor based on biocompatible conductive redox chitosan-ferrocene/gold nanoparticles matrix, Biosens. Bioelectron. 25(2009) 852–857.

[35] J. Jung, A. Solanki, K.A. Memoli, K. Kamei, H. Kim, M.A. Drahl, L.J. Williams, H.R. Tseng, K. Lee, Selective inhibition of human brain tumor cells through multifunctional quantum-dot-based siRNA delivery, Angew. Chem. Int. Ed. 49 (2010) 103–107.

[36] D.C. Marcano, D.V. Kosynkin, J.M. Berlin, A. Sinitskii, Z. Sun, A. Slesarev, L.B. Alemany, W. Lu, J.M. Tour, Improved synthesis of graphene oxide, ACS Nano 4 (2010) 4806–4814.

[37] K.C. Grabar, R.G. Freeman, M.B. Hommer, M.J. Natan, Preparation and Characterization of Au Colloid Monolayers, Anal. Chem. 67 (1995) 735–743.

[38] Z. She, K. Topping, M.H. Shamsi, N. Wang, N.W. Chan, H.B. Kraatz, Investigation of the utility of complementary electrochemical detection techniques to examine the in vitro affinity of bacterial flagellins for a toll-like receptor 5 biosensor, Anal. Chem. 87(2015) 4218–24.

[39] C. Xiang, R. Li, B. Adhikari, Z. She, Y. Li, H.-B. Kraatz, Sensitive electrochemical detection of *Salmonella* with chitosan–gold nanoparticles composite film, Talanta 140 (2015) 122–127.

[40] Y. Zou, Q. Wang, C. Xiang, Z. She, H. Chu, S. Qiu, F. Xu, S. Liu, C. Tang, L. Sun, One-pot synthesis of ternary polypyrrole–Prussian-blue–graphene-oxide hybrid composite as electrode material for high-performance supercapacitors, Electrochim. Acta 188 (2016) 126–134.

[41] M. Naebe, J. Wang, A. Amini, H. Khayyam, N. Hameed, L.H. Li, Y. Chen, B. Fox, Mechanical property and structure of covalent functionalised graphene/epoxy nanocomposites, Sci. Rep. 4 (2014) 4375.

[42] S.M. Singh Chauhan, S. Mishra, Use of graphite oxide and graphene oxide as catalysts in the synthesis of dipyrromethane and calix[4]pyrrole, Molecules 16 (2011) 7256–7266.

[43] S. Saha, M. Jana, P. Samanta, N.C. Murmu, T. Kuila, In situ preparation of a SAC-RGO@Ni electrode by electrochemical functionalization of reduced graphene oxide using sulfanilic acid azocromotrop and its application in asymmetric supercapacitors, J. Mater. Chem. A 3(2015) 19461–19468.

[44] R.A. Naikoo, R. Tomar, Fabrication of a novel Zeolite-X/Reduced graphene oxide/Polypyrrole nanocomposite and its role in sensitive detection of CO, Mater. Chemi. Phy. 211 (2018) 225–233.

[45] A. Ahmad, F. Syed, M. Imran, A.U. Khan, K. Tahir, Z.U.H. Khan, Q. Yuan, Phytosynthesis and antileishmanial activity of gold nanoparticles by maytenus royleanus, J. Food Biochem. 40(2016) 420–427.

[46] Z. Wang, X. Zhang, X. Liu, M. Lv, K. Yang, J. Meng, Co-gelation synthesis of porous graphitic carbons with high surface area and their applications, Carbon 49(2011) 161–169.

[47] F. Zou, H. Zhou, D.Y. Jeong, J. Kwon, S.U. Eom, T.J. Park, S.W. Hong, J. Lee, Wrinkled surface-mediated antibacterial activity of graphene oxide nanosheets, ACS Appl. Mater. Interfaces 9(2017) 1343–1351.

[48] Y. Liu, M.K. Wang, F. Zhao, Z.H. Guo, H.J. Chen, S.J. Dong, Direct electron transfer and electrocatalysis of microperoxidase immobilized on nanohybrid film,

J. Electroanal. Chem. 581(2005) 1–10.

[49] N. Elgrishi, K.J. Rountree, B.D. McCarthy, E.S. Rountree, T.T. Eisenhart, J.L. Dempsey, A practical beginner's guide to cyclic voltammetry, J. Chem. Edu. 95 (2017) 197–206.

[50] J. Wang, J. Gao, D. Liu, D. Han, Z. Wang, Phenylboronic acid functionalized gold nanoparticles for highly sensitive detection of *Staphylococcus aureu*s, Nanoscale, 4(2012)451–454.

[51] J. Lu, T.L. Gerke, H.Y. Buse, N.J. Ashbolt, Development of an Escherichia coli K12-specific quantitative polymerase chain reaction assay and DNA isolation suited to biofilms associated with iron drinking water pipe corrosion products, J Water Health 12 (2014) 763–771.

[52] I. Lee, S. Jun, Simultaneous detection of E. coli K12 and S. aureus Using a continuous flow multijunction biosensor, J. Food Sci. 81 (2016) N1530–N1536.

[53] K. Miyanaga, T. Hijikata, C. Furukawa, H. Unno, Y. Tanji, Detection of *Escherichia coli* in the sewage influent by fluorescent labeled T4 phage, Biochem. Eng. J. 29 (2006) 119–124.

[54] D.J. You, K.J. Geshell, J.Y. Yoon, Direct and sensitive detection of foodborne pathogens within fresh produce samples using a field-deployable handheld device, Biosens. Bioelectron. 28(2011) 399–406.

[55] N. Massad-Ivanir, G. Shtenberg, T. Zeidman, E. Segal, Construction and characterization of porous SiO_2/hydrogel hybrids as optical biosensors for rapid detection of bacteria, Adv. Funct. Mater. 20(2010) 2269–2277.

[56] J.C. Pyun, H. Beutel, J.U. Meyer, H.H. Ruf, Development of a biosensor for E. coli based on a flexural plate wave (FPW) transducer, Biosen. Bioelectron. 13 (1998) 839–845.

Graphical Abstract

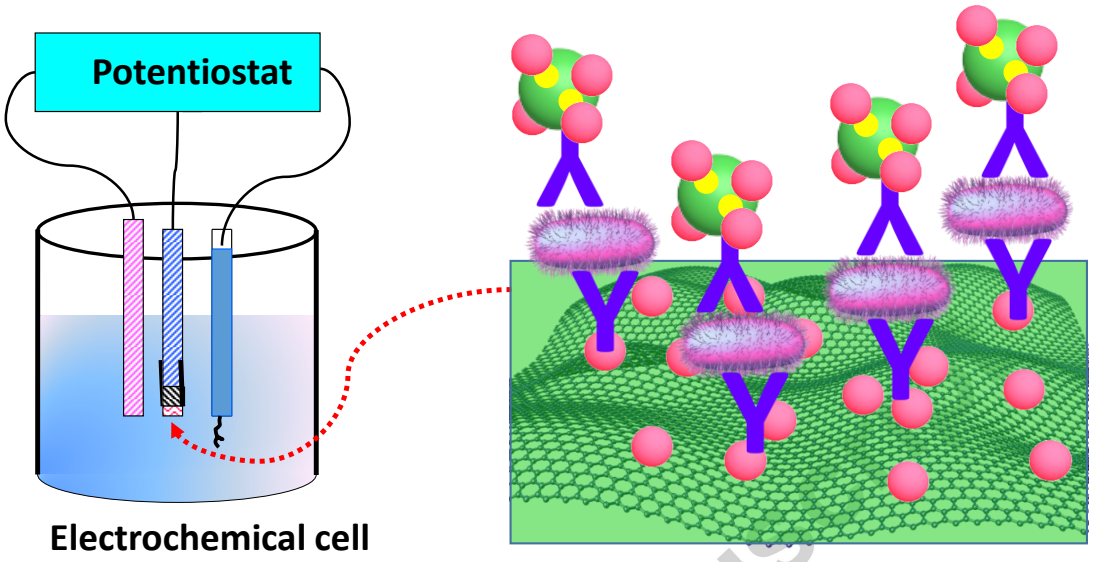

Highlights

- Gold nanoparticles were dispersed on the polypyrrole surface uniformly.
- The high conductive and biocompatible PPy-rGO/AuNPs nanocomposite was used as an interface to immobilize antibodies.
- Ferrocene doped polypyrrole-gold nanoparticles composite was used to generate current signal.
- An enzyme-free sandwich immunosensor was constructed with good analytical performance.